

Pamela W. Schaefer, MD
P. Ellen Grant, MD
R. Gilberto Gonzalez, MD,
PhD

Index terms:

Brain, diffusion
Brain, infarction, 10.781
Brain, infection, 10.20
Brain, injuries, 10.41, 10.42
Brain, ischemia, 10.781
Brain, MR, 10.12141, 10.12144
Brain neoplasms, 10.31, 10.32
Sclerosis, multiple, 10.871
State of the Art

Radiology 2000; 217:331–345

Abbreviations:

ADC = apparent diffusion coefficient
CSF = cerebrospinal fluid
DW = diffusion weighted

¹ From the Neuroradiology Division, Massachusetts General Hospital, GRB 285, Fruit St, Boston, MA 02114-2696. Received April 30, 1999; revision requested July 14; revision received November 8; accepted November 15. **Address correspondence to** R.G.G. (e-mail: rggonzalez@partners.org).

© RSNA, 2000

Diffusion-weighted MR Imaging of the Brain¹

Diffusion-weighted magnetic resonance (MR) imaging provides image contrast that is different from that provided by conventional MR techniques. It is particularly sensitive for detection of acute ischemic stroke and differentiation of acute stroke from other processes that manifest with sudden neurologic deficits. Diffusion-weighted MR imaging also provides adjunctive information for other cerebral diseases including neoplasms, intracranial infections, traumatic brain injury, and demyelinating processes. Because stroke is common and in the differential diagnosis of most acute neurologic events, diffusion-weighted MR imaging should be considered an essential sequence, and its use in most brain MR studies is recommended.

Diffusion-weighted (DW) magnetic resonance (MR) imaging provides potentially unique information on the viability of brain tissue. It provides image contrast that is dependent on the molecular motion of water, which may be substantially altered by disease. The method was introduced into clinical practice in the middle 1990s, but because of its demanding MR engineering requirements—primarily high-performance magnetic field gradients—it has only recently undergone widespread dissemination. The primary application of DW MR imaging has been in brain imaging, mainly because of its exquisite sensitivity to ischemic stroke—a common condition that appears in the differential diagnosis in virtually all patients who present with a neurologic complaint.

Because DW MR imaging uses fast (echo-planar) imaging technology, it is highly resistant to patient motion, and imaging time ranges from a few seconds to 2 minutes. As a consequence, DW MR imaging has assumed an essential role in the detection of acute brain infarction and in the differentiation of acute infarction from other disease processes. DW MR imaging is also assuming an increasingly important role in the evaluation of many other intracranial disease processes.

BASIC CONCEPTS OF DW MR IMAGING

In this section, the basic concepts involved in DW MR imaging will be briefly reviewed. For more detailed descriptions of the physics of DW imaging, a number of excellent reviews (1–5) are available. Stejskal and Tanner (6) provided an early description of a DW sequence in 1965. They used a spin-echo T2-weighted pulse sequence with two extra gradient pulses that were equal in magnitude and opposite in direction. This sequence enabled the measurement of net water movement in one direction at a time. To measure the rate of movement along one direction, for example the x direction, these two extra gradients are equal in magnitude but opposite in direction for all points at the same x location. However, the strength of these two balanced gradients increases along the x direction. Therefore, if a voxel of tissue contains water that has no net movement in the x direction, the two balanced gradients cancel each other out. The resultant signal intensity of that voxel is equal to its signal intensity on an image obtained with the same sequence without the DW gradients. However, if water molecules have a net movement in the x direction (eg, due to diffusion), they are subjected to the first gradient pulse at one x location and the second pulse at a different x location. The two gradients are no longer equal in magnitude and no longer cancel. The difference in gradient pulse magnitude is proportional to the net displacement in the x direction that occurs between the two gradient pulses, and faster-moving water protons undergo a larger net dephasing. The resultant signal intensity of a voxel of tissue containing moving protons is equal to its signal

intensity on a T2-weighted image decreased by an amount related to the rate of diffusion.

The signal intensity (SI) of a voxel of tissue is calculated as follows:

$$SI = SI_0 \times \exp(-b \times D), \quad (1)$$

where SI_0 is the signal intensity on the T2-weighted (or $b = 0 \text{ sec/mm}^2$) image, the diffusion sensitivity factor b is equal to $\gamma^2 G^2 \delta^2 (\Delta - \delta/3)$, and D is the diffusion coefficient. γ is the gyromagnetic ratio; G is the magnitude of, δ the width of, and Δ the time between the two balanced DW gradient pulses.

According to Fick's law, true diffusion is the net movement of molecules due to a concentration gradient. With MR imaging, molecular motion due to concentration gradients cannot be differentiated from molecular motion due to pressure gradients, thermal gradients, or ionic interactions. Also, with MR imaging we do not correct for the volume fraction available or the increases in distance traveled due to tortuous pathways. Therefore, when measuring molecular motion with DW imaging, only the apparent diffusion coefficient (ADC) can be calculated. The signal intensity of a DW image is best expressed as

$$SI = SI_0 \times \exp(-b \times \text{ADC}). \quad (2)$$

With the development of high-performance gradients, DW imaging can be performed with an echo-planar spin-echo T2-weighted sequence. With the original spin-echo T2-weighted sequence, even minor bulk patient motion was enough to obscure the much smaller molecular motion of diffusion. The substitution of an echo-planar spin-echo T2-weighted sequence markedly decreased imaging time and motion artifacts and increased sensitivity to signal changes due to molecular motion. As a result, the DW sequence became clinically feasible to perform. Other methods of performing DW MR imaging without echo-planar gradients have also been developed. These include DW sequences based on a single-shot gradient and spin-echo or single-shot fast spin-echo techniques (7,8). "Line-scan" DW and spiral DW sequences have also been developed (9–12).

In the brain, apparent diffusion is not isotropic (the same in all directions); it is anisotropic (varies in different directions), particularly in white matter. The cause of the anisotropic nature of white matter is not completely understood, but increasing anisotropy has also been

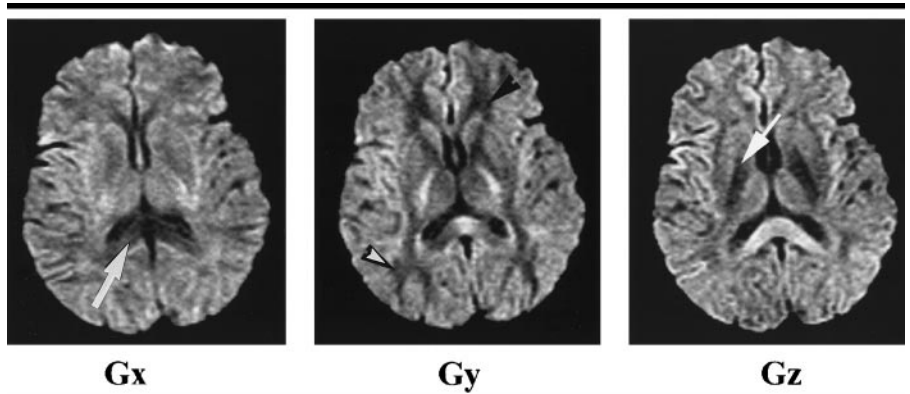


Figure 1. Anisotropic nature of diffusion in the brain. Transverse DW MR images ($b = 1,000 \text{ sec/mm}^2$; effective gradient, 14 mT/m; repetition time, 7,500 msec; minimum echo time; matrix, 128×128 ; field of view, $200 \times 200 \text{ mm}$; section thickness, 6 mm with 1-mm gap) with the diffusion gradients applied along the x (G_x , left), y (G_y , middle), and z (G_z , right) axes demonstrate anisotropy. The signal intensity decreases when the white matter tracts run in the same direction as the DW gradient because water protons move preferentially in this direction. Note that the corpus callosum (arrow on left image) is hypointense when the gradient is applied in the x (right-to-left) direction, the frontal and posterior white matter (arrowheads) are hypointense when the gradient is applied in the y (anterior-to-posterior) direction, and the corticospinal tracts (arrow on right image) are hypointense when the gradient is applied in the z (superior-to-inferior) direction.

noted in the developing brain before T1- and T2-weighted imaging or histologic evidence of myelination becomes evident (13,14). It is likely that in addition to axonal direction and myelination, other physiologic processes, such as axolemmic flow, extracellular bulk flow, capillary blood flow, and intracellular streaming, may contribute to white matter anisotropy. The anisotropic nature of diffusion in the brain can be appreciated by comparing images obtained with DW gradients applied in three orthogonal directions (Fig 1). In each of the images, the signal intensity is equal to the signal intensity on echo-planar T2-weighted images decreased by an amount related to the rate of diffusion in the direction of the applied gradients. Images obtained with gradient pulses applied in one direction at a time are combined to create DW images or ADC maps. The ADC is actually a tensor quantity or a matrix:

$$\text{ADC} = \begin{bmatrix} \text{ADC}_{xx} & \text{ADC}_{xy} & \text{ADC}_{xz} \\ \text{ADC}_{yx} & \text{ADC}_{yy} & \text{ADC}_{yz} \\ \text{ADC}_{zx} & \text{ADC}_{zy} & \text{ADC}_{zz} \end{bmatrix}. \quad (3)$$

The diagonal elements of this matrix can be combined to give information about the magnitude of the apparent diffusion: $(\text{ADC}_{xx} + \text{ADC}_{yy} + \text{ADC}_{zz})/3$.

The off-diagonal elements provide information about the interactions between the x, y, and z directions. For example, ADC_{yx} gives information about the correlation between displacements in the x and y directions (4). Images display-

ing the magnitude of the ADC are used in clinical practice.

DW gradient pulses are applied in one direction at a time. The resultant image has information about both the direction and the magnitude of the ADC (Fig 1). To create an image that is related only to the magnitude of the ADC, at least three of these images must be combined. The simplest method is to multiply the three images created with the DW gradient pulses applied in three orthogonal directions. The cube root of this product is the DW image (Fig 2). It is important to understand that the DW image has T2-weighted contrast as well as contrast due to differences in ADC. To remove the T2-weighted contrast, the DW image can be divided by the echo-planar spin-echo T2-weighted (or $b = 0 \text{ sec/mm}^2$) image to give an "exponential image" (Fig 3). Alternatively, an ADC map, which is an image whose signal intensity is equal to the magnitude of the ADC, can be created (Fig 4).

Instead of obtaining images with $b = 0 \text{ sec/mm}^2$ and with $b = 1,000 \text{ sec/mm}^2$ and solving for ADC using Equation (2), one usually determines the ADC graphically. This is accomplished by obtaining two image sets, one with a very low but nonzero b value and one with $b = 1,000 \text{ sec/mm}^2$. By plotting the natural logarithm of the signal intensity versus b for these two b values, the ADC can be determined from the slope of this line.

For our clinical studies, the DW image,

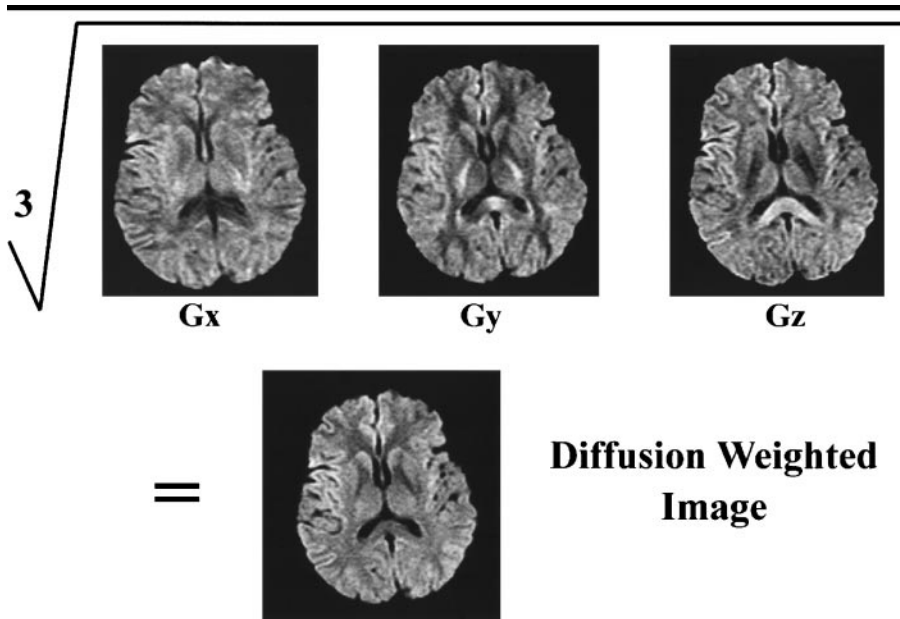


Figure 2. Calculation of signal intensity on an isotropic DW image ($b = 1,000 \text{ sec/mm}^2$; effective gradient, 14 mT/m; repetition time, 7,500 msec; minimum echo time; matrix, 128×128 ; field of view, $400 \times 200 \text{ mm}$; section thickness, 6 mm with 1-mm gap). The signal intensities of the three transverse images (G_x , G_y , and G_z), each with a diffusion gradient applied in one of three orthogonal directions, are multiplied together. Here the DW gradients were applied along the x, y, and z axes. The signal intensity of the isotropic DW image (bottom) is essentially the cube root of the signal intensities of these three images multiplied together. Note that both T2-weighted contrast and the rate of diffusion contribute to the signal intensity of the isotropic DW image.

exponential image, ADC map, and echo-planar spin-echo T2-weighted images are routinely available for review (Fig 4). Because the ADC values of gray and white matter are similar, typically there is no contrast between gray and white matter on the exponential image or ADC map. The contrast between gray and white matter seen on the DW image is due to T2-weighted contrast. This residual T2 component on the DW image makes it important to view either the exponential image or ADC map in conjunction with the DW image. In lesions such as acute stroke, the T2-weighted and DW effects both cause increased signal intensity on the DW image. Therefore, we have found that we identify regions of decreased diffusion best on DW images. The exponential image and ADC maps are used to exclude "T2 shine through" as the cause of increased signal intensity on DW images. The exponential image and ADC map are useful for detecting areas of increased diffusion that may be masked by T2 effects on the DW image.

CLINICAL APPLICATIONS

The Table provides a summary of DW and ADC imaging findings, as well as the characteristic ADC and causes, for a variety of disease entities.

Ischemic Stroke

Theory of restricted diffusion in acute stroke.—Within minutes after the onset of ischemia, a profound restriction in water diffusion occurs in affected brain tissue (15–18). The biophysical basis of this change is not completely clear. One likely important contributor is cytotoxic edema. Cytotoxic edema induced with acute hyponatremic encephalopathy (without ischemia) is associated with restricted diffusion (19). Furthermore, when decreased ADCs were present in early ischemia in rat brain tissue, there was a reduction in Na^+/K^+ adenosine triphosphatase activity without a significant increase in brain water (16). In addition, ouabain, an inhibitor of Na^+/K^+ adenosine triphosphatase, was associated with a reduction in ADC in rat cortex (20). These findings have led to the predominant theory for the restriction of water diffusion in stroke: Ischemia causes disruption of energy metabolism, leading to failure of the Na^+/K^+ adenosine triphosphatase pump and other ionic pumps. This leads to loss of ionic gradients and a net translocation of water from the extracellular to the intracellular compart-

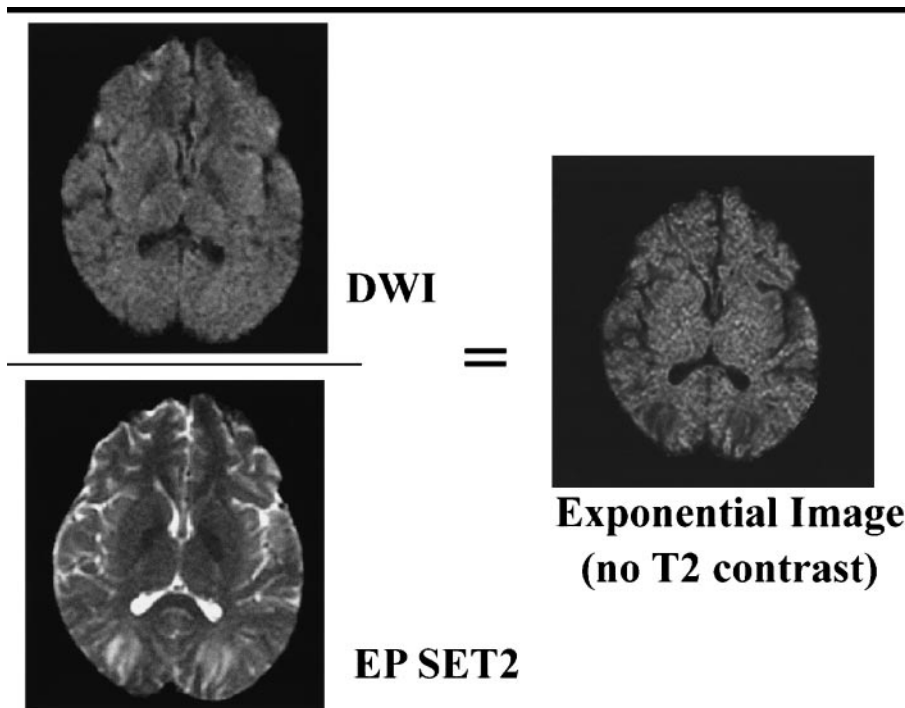


Figure 3. Removal of T2-weighted contrast. To remove the T2-weighted contrast in the isotropic transverse DW image ($b = 1,000 \text{ sec/mm}^2$; effective gradient, 14 mT/m; repetition time, 7,500 msec; minimum echo time; matrix, 128×128 ; field of view, $200 \times 200 \text{ mm}$, section thickness, 6 mm with 1-mm gap), the transverse DW image (DWI) is divided by the transverse echo-planar spin-echo T2-weighted (EP SET2) image. The resultant image is called the exponential image because its signal intensity is exponentially related to the ADC.

DW MR Imaging Characteristics of Various Disease Entities

Disease	MR Signal Intensity		ADC	Cause
	DW Image	ADC Image		
Acute stroke	High	Low	Restricted	Cytotoxic edema
Chronic stroke	Variable	High	Elevated	Gliosis
Hypertensive encephalopathy	Variable	High	Elevated	Vasogenic edema
Cyclosporin toxicity	Variable	High	Elevated	Vasogenic edema
Hyperperfusion after carotid endarterectomy	Variable	High	Elevated	Vasogenic edema
HIV encephalopathy	Variable	High	Elevated	Vasogenic edema
Intraaxial mass				
Necrotic center	Variable	High	Elevated	Increased free water
Solid tumor	Variable	Variable	Variable	Depends on cellularity
Arachnoid cyst	Low	High	Elevated	Free water
Epidermoid mass	High	Low*	Restricted*	Cellular tumor
Pyogenic infection	High	Low	Restricted	Viscosity
Herpes encephalitis	High	Low	Restricted	Cytotoxic edema
Creutzfeldt-Jakob syndrome	High	Low	Restricted	Unknown
Diffuse axonal injury				
Majority of cases	High	Low	Restricted	Cytotoxic edema
Minority of cases	Variable	High	Elevated	Vasogenic edema
Hemorrhage				
Oxyhemoglobin	High	Low	Restricted	Intracellular
Deoxyhemoglobin	Low	Unknown†	Unknown†	Unknown†
Intracellular methemoglobin	Low	Unknown†	Unknown†	Unknown†
Extracellular methemoglobin	High	High	Elevated	Extracellular
Hemosiderin	Low	Unknown†	Unknown†	Unknown†
Multiple sclerosis				
Most acute lesions	Variable	High	Elevated	Vasogenic edema
A few acute lesions	High	Low	Restricted	Unknown
Chronic lesions	Variable	High	Elevated	Gliosis, neuronal loss

* Relative to that of cerebrospinal fluid (CSF).

† The ADC usually cannot be calculated.

ment, where water mobility is relatively more restricted.

There are additional factors. With cellular swelling, there is a reduction in the volume of extracellular space (21). A decrease in the diffusion of low-molecular-weight tracer molecules has been demonstrated in animal models (22,23), which suggests that the increased tortuosity of extracellular space pathways contributes to restricted diffusion in acute ischemia. Furthermore, there are substantial reductions in ADCs in intracellular metabolites in ischemic rat brain (24–26). Proposed explanations are increased intracellular viscosity due to dissociation of microtubules and fragmentation of other cellular components or increased tortuosity of the intracellular space and decreased cytoplasmic mobility. It is worth bearing in mind that the normal steady-state function of these structures requires energy and uses adenosine triphosphate. Other factors such as temperature (27,28) and cell membrane permeability (29,30) play a minor role in explaining the reduction in ADC in acutely ischemic tissue.

Time course of lesion evolution in acute stroke.—In animals, restricted diffusion associated with acute ischemia has been detected as early as 10 minutes to 2 hours after vascular occlusion (17,18,31–35).

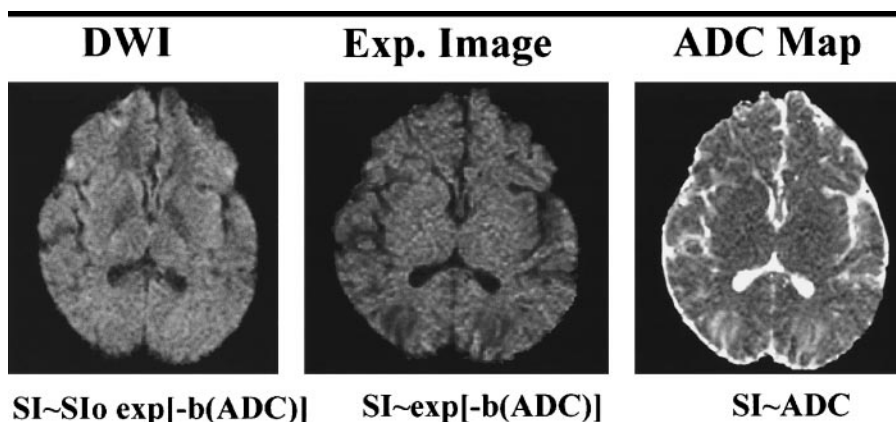


Figure 4. Creation of an ADC map. One method of creating an ADC map is to mathematically manipulate the exponential (*Exp.*) image. The appearances on the transverse DW image (*DWI*), exponential image, and ADC map, as well as the corresponding mathematic expressions for their signal intensities, are shown. Image parameters are $b = 1,000 \text{ sec/mm}^2$; effective gradient, 14 mT/m; repetition time, 7,500 msec; minimum echo time; matrix, 128×128 ; field of view, $200 \times 200 \text{ mm}$; section thickness, 6 mm with 1-mm gap. *SI* = signal intensity, *SIo* = signal intensity on T2-weighted image.

The ADCs measured at these times are approximately 16%–68% below those of normal tissue. In animals, ADCs pseudo-normalize (ie, are similar to those of normal brain tissue, but the tissue is infarcted) at approximately 2 days and are elevated thereafter.

In adult humans, the time course is

more prolonged (Fig 5) (36–39). We have observed restricted diffusion associated with acute ischemia 30 minutes after a witnessed ictus. The ADC continues to decrease and is most reduced at 8–32 hours. The ADC remains markedly reduced for 3–5 days. This decreased diffusion is markedly hyperintense on DW

images (which are generated with a combination of T2-weighted and DW imaging) and hypointense on ADC images. The ADC returns to baseline at 1–4 weeks. This most likely reflects persistence of cytotoxic edema (associated with decreased diffusion) and development of vasogenic edema and cell membrane disruption, leading to increased extracellular water (associated with increased diffusion). At this point, an infarction is usually mildly hyperintense due to the T2 component on the DW images and isointense on the ADC images. Thereafter, diffusion is elevated as a result of continued increase in extracellular water, tissue cavitation, and gliosis. This elevated diffusion is characterized by slight hypointensity, isointensity, or hyperintensity on the DW images (depending on the strength of the T2 and diffusion components) and increased signal intensity on ADC maps.

The time course does not always conform to the aforementioned outline. With early reperfusion, pseudonormalization (return to baseline of the ADC reduction associated with acute ischemic stroke) may occur at a much earlier time—as early as 1–2 days in humans given intravenous recombinant tissue plasminogen activator less than 3 hours after stroke onset (40). Furthermore, Nagesh et al (41) demonstrated that although the mean ADC of an ischemic lesion is depressed within 10 hours, different zones within an ischemic region may demonstrate low, pseudonormal, or elevated ADCs, suggesting different temporal rates of tissue evolution toward infarction. Despite these variations, tissue characterized by an initial reduction in ADC nearly always undergoes infarction in humans.

DW and perfusion-weighted MR imaging for assessment of stroke evolution.—The combination of perfusion-weighted and DW MR imaging may provide more information than would either technique alone. Perfusion-weighted imaging involves the detection of a decrease in signal intensity as a result of the susceptibility or T2* effects of gadolinium during the passage of a bolus of a gadolinium-based contrast agent through the intracranial vasculature (42,43). A variety of hemodynamic images may be constructed from these data, including relative cerebral blood volume, relative cerebral blood flow, mean transit time, and time-to-peak maps (43–47).

In the context of arterial occlusion, brain regions with decreased diffusion and perfusion are thought to represent nonviable tissue or the core of an infarction

(31,32,34,39,48–51). The majority of stroke lesions increase in volume on DW images, with the maximum volume achieved at 2–3 days.

When most patients with acute stroke are evaluated with both DW and perfusion-weighted MR imaging, their images usually demonstrate one of three patterns (39,49–52): A lesion is smaller on DW images than the same lesion is on perfusion-weighted images; a lesion on DW images is equal to or larger than that on perfusion-weighted images; or a lesion is depicted on DW images but is not demonstrable on perfusion-weighted images. In large-vessel stroke lesions (such as in the proximal portion of the middle cerebral artery), the abnormality as depicted on perfusion-weighted images is frequently larger than the lesion as depicted on DW images. The peripheral region, characterized by normal diffusion and decreased perfusion, usually progresses to infarction unless there is early reperfusion. Thus, in the acute setting, perfusion-weighted imaging in combination with DW imaging helps identify an operational “ischemic penumbra” or area at risk for infarction (Fig 6).

On the other hand, in small-vessel infarctions (perforator infarctions and distal middle cerebral artery infarctions), the initial lesion volumes on perfusion-weighted and DW images are usually similar, and the diffusion-weighted image lesion volume increases only slightly with time. A lesion larger on DW images than on perfusion-weighted images or a lesion visible on DW images but not on perfusion-weighted images usually occurs with early reperfusion. In this situation, the lesion on DW images usually does not change substantially over time.

In animals treated with neuroprotective agents after occlusion of the middle cerebral artery, the increase in stroke lesion volume on serial DW images is reduced (53,54). This effect has not been convincingly demonstrated in humans.

Reversibility of ischemic lesions on DW images.—In animal models of ischemia, both a time threshold and an ADC threshold for reversibility have been demonstrated. In general, when the middle cerebral artery in animals is temporarily occluded for an hour or less, the diffusion lesion size markedly decreases or resolves; however, when the middle cerebral artery is occluded for 2 hours or more, the lesion size remains the same or increases (17,34,55–57). Hasegawa et al (55) demonstrated that after 45 minutes

of temporary occlusion of the middle cerebral artery in rats, diffusion lesions are partially or completely reversible when the difference in ADC values between the ischemic region and a contralateral homologous nonischemic region is not greater than a threshold of -0.25×10^{-5} cm²/sec. When the ADC difference is greater than this threshold, the lesion nearly always becomes completely infarcted. Similarly Dardzinski et al (58) demonstrated a threshold ADC of 0.55×10^{-3} mm²/sec at 2 hours in a permanent-occlusion rat model.

In humans, reversibility of ischemic lesions is rare. To our knowledge, only one case has been reported in the literature (59), and we have observed reversibility of only one ischemic lesion in over 2,000 patients imaged in our clinical practice (Fig 7). That patient was treated with intravenous recombinant tissue plasminogen activator 2 hours after symptom onset, and the initial ADC was approximately 20% below that of contralateral homologous nonischemic brain tissue. In humans, neither a threshold time nor a threshold ADC for reversibility have been established.

DW imaging reliability in acute stroke.—Conventional computed tomography (CT) and MR imaging cannot be used to reliably detect infarction at the earliest time points. The detection of hypoattenuation on CT scans and hyperintensity on T2-weighted MR images requires a substantial increase in tissue water. For infarctions imaged within 6 hours after stroke onset, reported (60,61) sensitivities are 38%–45% for CT and 18%–46% for MR imaging. For infarctions imaged within 24 hours, the authors of one study (62) reported a sensitivity of 58% for CT and 82% for MR imaging.

DW images are very sensitive and specific for the detection of hyperacute and acute infarctions, with a sensitivity of 88%–100% and a specificity of 86%–100% (59,60,63). A lesion with decreased diffusion is strongly correlated with irreversible infarction. Acute neurologic deficits suggestive of stroke but without restricted diffusion are typically due to transient ischemic attack, peripheral vertigo, migraine, seizures, intracerebral hemorrhage, dementia, functional disorders, amyloid angiopathy, and metabolic disorders (59,60,63).

Although, after 24 hours, infarctions usually can be detected as hypoattenuating lesions on CT and hyperintense lesions on T2-weighted and fluid-attenuated inversion recovery MR images, DW imaging is useful in this setting, as well.

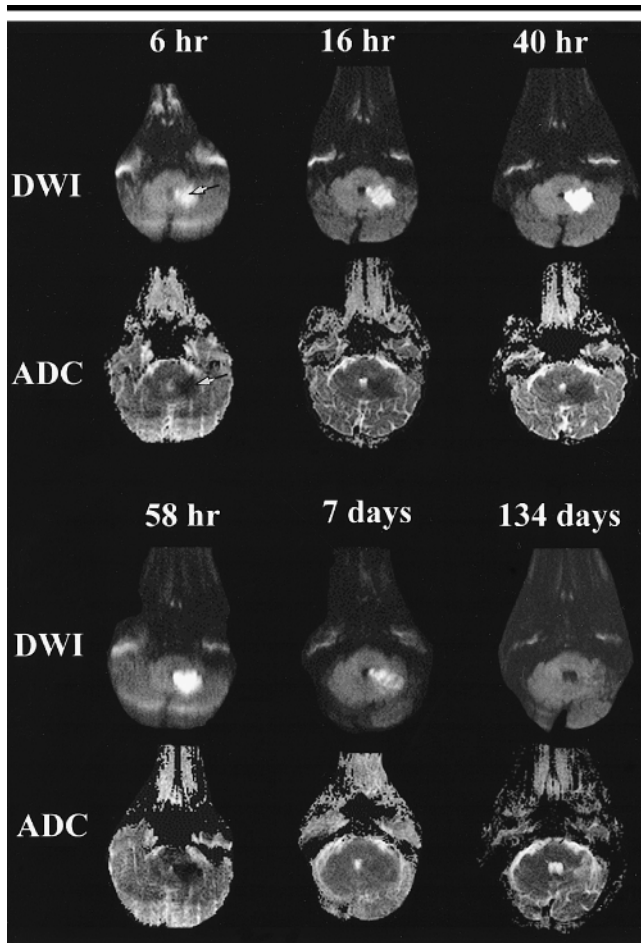


Figure 5. Time course of an ischemic infarction. Images demonstrate the evolution of an ischemic infarction involving the left cerebellar hemisphere and left middle cerebellar peduncle. Both transverse DW images (*DWI*; $b = 1,000 \text{ sec/mm}^2$; effective gradient, 14 mT/m; repetition time msec/echo time msec, 6,000/108; matrix, 256×128 ; field of view, $400 \times 200 \text{ mm}$; section thickness, 6 mm with 1-mm gap) and transverse ADC maps are displayed. The patient underwent MR imaging 6 hours after the onset of acute neurologic symptoms. At 6 hours, the lesion (arrows) is hyperintense on the DW images and hypointense on the corresponding ADC map. The lesion becomes progressively more hyperintense on DW images, reaching its maximum hyperintensity at the 58-hour time point, when it also reaches its maximum hypointensity on ADC maps. At 7 days, there is ongoing resolution of the lesion on both DW images and ADC maps. By 134 days, there is subtle hypointensity on the DW image and hyperintensity on the ADC images.

Older patients commonly have hyperintense abnormalities on T2-weighted images that may be indistinguishable from acute lesions. However, acute infarctions are hyperintense on DW images and hypointense on ADC maps, whereas chronic foci are usually isointense on DW images and hyperintense on ADC maps due to elevated diffusion (Fig 8). In one study (64) in which there were indistinguishable acute and chronic white matter lesions on T2-weighted images in 69% of patients, the sensitivity and specificity of DW imaging for detection of

acute subcortical infarction were 94.9% and 94.1%, respectively.

False-negative DW images have been reported in patients with very small lacunar brainstem or deep gray nuclei infarction (60,63,65). Some of these lesions were seen on follow-up DW images, and others were presumed to be present on the basis of clinical deficits. False-negative DW images also occur in patients with regions of decreased per-

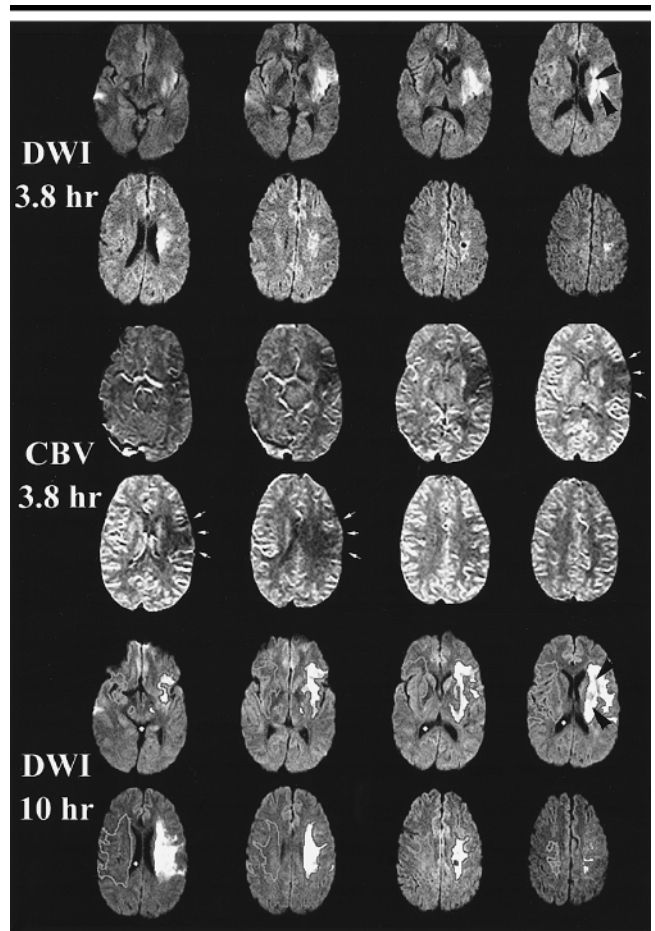


Figure 6. Diffusion-perfusion mismatch after left middle cerebral artery stroke. The patient was imaged 3.8 hours after a witnessed sudden onset of a right hemiparesis. Transverse DW images (*DWI*; $b = 1,000 \text{ sec/mm}^2$; effective gradient, 14 mT/m; 6,000/108; matrix, 256×128 ; field of view, $400 \times 200 \text{ mm}$; section thickness, 6 mm with 1-mm gap) demonstrate hyperintensity in the subcortical region, including in the lenticular nucleus and corona radiata (arrowheads, right-hand image in top row). Transverse cerebral blood volume (*CBV*) images (spin-echo echo-planar technique; 0.2 mmol/kg gadopentetate dimeglumine [Magnevist; Berlex Laboratories, Wayne, NJ]; 51 images per section; 1,500/75; matrix, 256×128 ; field of view, $400 \times 200 \text{ mm}$; section thickness, 6 mm with 1-mm gap) demonstrate decreased dynamic cerebral blood volume in the region of hyperintensity on the DW images. However, there are areas of abnormal cerebral blood volume (arrows) that appear relatively normal on the DW study. Follow-up study performed 10 hours after the onset of symptoms demonstrates an increase in the size of the DW imaging abnormality (arrowheads, right-hand image in fifth row) as it extends into the region of brain that was previously normal on DW images but abnormal on cerebral blood volume images.

fusion (increased mean transit time and decreased relative cerebral blood flow), which are hyperintense on follow-up DW images; in other words, these patients initially had regions characterized by ischemic but viable tissue that progressed to infarction. These findings stress the importance of obtaining early follow-up images in patients with normal DW images and persistent stroke-like deficits, so that infarctions or areas

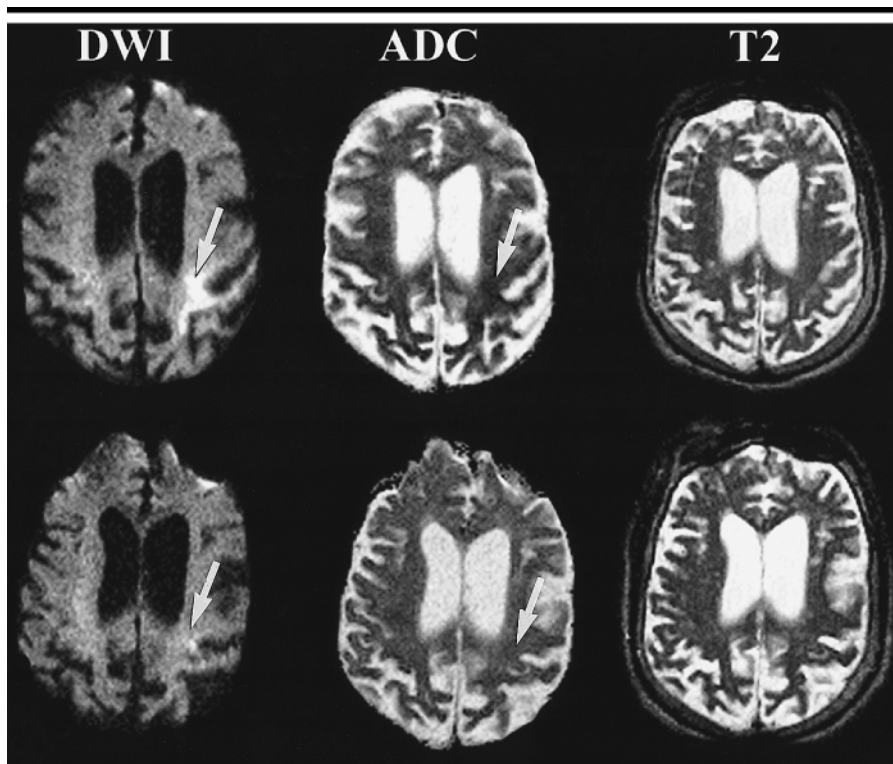


Figure 7. Reversible ischemic lesion. Top: The patient was imaged approximately 2 hours after the onset of a witnessed acute neurologic deficit. Top left: Transverse DW image (DWI; $b = 1,000$ sec/mm²; effective gradient, 14 mT/m; 6,000/108; matrix, 256 × 128; field of view, 400 × 200 mm; section thickness, 6 mm with 1-mm gap) shows an area of hyperintensity (arrow) in the left posterior frontal and anterior parietal lobes. Top middle: A region of hypointensity (arrow) corresponding to this area is seen on the transverse ADC image (arrow). Top right: No definite abnormality is seen on the transverse fast spin-echo T2-weighted MR image (4,000/104; echo train length, eight; matrix, 256 × 192; field of view, 200 × 200 mm; section thickness, 5 mm with 1-mm gap; one signal acquired). The patient was treated with intravenous recombinant tissue plasminogen activator, with resolution of the neurologic symptoms. Bottom: Follow-up images obtained 3 days later demonstrate near interval resolution of the abnormalities on the 2-hour DW image and ADC map. No definite lesion was identified on the follow-up T2-weighted image. Of note, the decrease in ADC was approximately 20% of the normal value. Lesions that become confirmed infarctions typically demonstrate a 50% reduction in ADC.

at risk for infarction are identified and treated as early as possible.

False-positive DW images have been reported in patients with a diagnosis other than acute infarction. These include cerebral abscess (with restricted diffusion on the basis of viscosity) and tumor (with restricted diffusion on the basis of dense cell packing). When these lesions are viewed on DW images in combination with other routine T1- and T2-weighted MR images, they can usually be differentiated from acute infarctions.

Correlation of DW MR imaging with clinical outcome.—DW MR imaging findings may reflect the severity of clinical neurologic deficits and help predict clinical outcome. Statistically significant correlations between the acute DW MR lesion volume and both acute and chronic neurologic assessment results, including

those of the National Institutes of Health Stroke Score Scale, the Canadian Neurologic Scale, the Barthel Index, and the Rankin Scale, have been demonstrated (39,51,66–68). This correlation is stronger in cases of cortical stroke and weaker in cases of penetrator artery stroke (39,66). Lesion location likely explains the variance; for example, a lesion in a major white matter tract may produce a more profound neurologic deficit than would a cortical lesion of the same size. There also is a weaker correlation between initial lesion volume and National Institutes of Health Stroke Score Scale measures in patients with a prior infarction. In addition, there is a significant correlation between the acute ADC ratio (lesion ADC to normal contralateral brain ADC) and chronic neurologic assessment scale scores (39,68). Perfusion-weighted image volumes also correlate with acute and chronic neuro-

logic assessment test results (51,67). In one study (51), patients who had lesion volumes on perfusion-weighted images that were larger than volumes on DW images (perfusion-diffusion mismatches) had worse outcomes and larger final infarct volumes. In another study (39), patients with early reperfusion had smaller final infarct volumes and better clinical outcomes. Because DW and perfusion-weighted MR imaging can help predict clinical outcome at very early time points, these techniques may prove to be valuable for the selection of patients for thrombolysis or administration of neuroprotective agents.

Neonatal hypoxic ischemic brain injury.—DW MR imaging is rapidly improving the evaluation of neonatal hypoxic ischemic encephalopathy and focal infarctions. Animal models of neonatal ischemia have demonstrated lesions on DW MR images as early as 1 hour after ligation of the carotid artery (69,70). In humans, within 1 day of birth, acute ischemic lesions not seen on routine CT or MR images are identified on DW MR images (71,72). When lesions are identified on conventional images, lesion conspicuity is increased and lesion extent is seen to be larger on DW MR images. In addition, lesions identified on the initial DW MR images are identified on follow-up conventional images and, therefore, help accurately predict the extent of infarction. This correlates with the finding in animals that areas of restricted diffusion correlate with areas of injury at autopsy.

Animal models have also demonstrated the evolution of neonatal hypoxic ischemic injury over time. In a rabbit model (70), ischemic lesions were seen first in the cortex, followed by the subcortical white matter, the ipsilateral basal ganglia, and the contralateral basal ganglia.

Thus, DW MR imaging is helping increase our understanding of the pathophysiology of neonatal ischemia. It allows timing of ischemic onset, provides earlier and more reliable detection of acute ischemic lesions, and allows differentiation of focal infarctions from more global hypoxic ischemic lesions. This information may provide a better early assessment of the long-term prognosis and may be important in the evaluation of new neuroprotective agents.

Transient ischemic attacks.—Nearly 50% of patients with transient ischemic attacks have lesions characterized by restricted diffusion (73,74). These lesions are usually small (<15-mm diameter), are

almost always in the clinically expected vascular territory, and are thought to represent markers of more widespread reversible ischemia. In one study (74), 20% of the lesions were not seen at follow-up; the lesions could have been reversible or, owing to atrophy, too small to see on conventional MR images. The information obtained from DW MR imaging changed the suspected localization of an ischemic lesion, as well as the suspected etiologic mechanism, in more than one-third of patients (74). In another study (73), statistically significant independent predictors for identification of these lesions on DW MR images included previous nonstereotypic transient ischemic attack, cortical syndrome, or an identified stroke mechanism, and the authors suggested an increased stroke risk in patients with these lesions. Early identification of patients with transient ischemic attack with increased risk of stroke and better identification of etiologic mechanisms is changing acute management and may affect patient outcome.

Other clinical stroke mimics.—These syndromes generally fall into two categories: (a) nonischemic lesions with no acute abnormality on routine or DW MR images or (b) vasogenic edema syndromes that mimic acute infarction on conventional MR images. Nonischemic syndromes with no acute abnormality identified on DW or conventional MR images and reversible clinical deficits include peripheral vertigo, migraines, seizures, dementia, functional disorders, amyloid angiopathy, and metabolic disorders (59,60,63). When a patient with these syndromes present, we can confidently predict that they are not undergoing infarction; they are spared unnecessary anticoagulation treatment and a stroke work-up.

Syndromes with potentially reversible vasogenic edema include eclampsia, hypertensive encephalopathy, cyclosporin toxicity, other posterior leukoencephalopathies, venous thrombosis, human immunodeficiency virus encephalopathy, and hyperperfusion syndrome after carotid endarterectomy (Fig 9). Patients with these syndromes frequently present with neurologic deficits that are suggestive of acute ischemic stroke or with neurologic deficits such as headache or seizure that are suggestive of vasogenic edema, but ischemic stroke is still a strong diagnostic consideration. Conventional MR imaging cannot help differentiate vasogenic edema from the cytotoxic edema associated with acute infarction. Cytotoxic edema produces

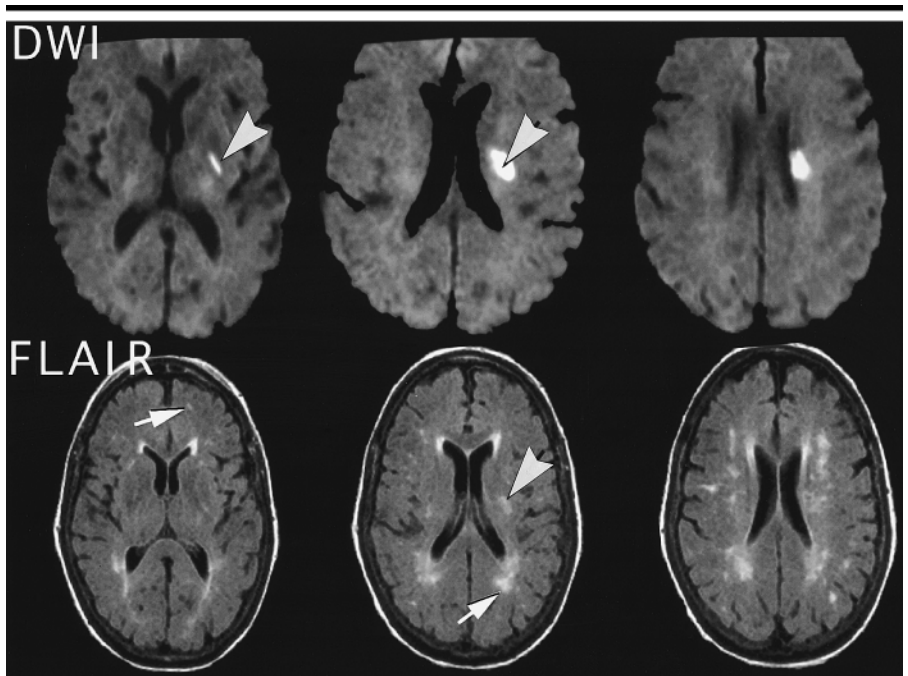


Figure 8. Differentiation of acute white matter infarction from nonspecific small-vessel ischemic changes. This patient had onset of symptoms 2 days prior to imaging. Top: Transverse DW images (*DWI*; $b = 1,000 \text{ sec/mm}^2$; effective gradient, 14 mT/m; 6,000/108; matrix, 256 × 128; field of view, 400 × 200 mm; section thickness, 6 mm with 1-mm gap) in the top row clearly demonstrate the acute infarction (arrowheads) in the putamen and corona radiata. Bottom: Fluid-attenuated inversion recovery (*FLAIR*) images (10,000/141; inversion time, 2,200 msec; echo train length, eight; matrix, 256 × 192; field of view, 240 × 240 mm; section thickness, 5 mm with 1-mm gap; one signal acquired) demonstrate multiple white matter lesions in which acute (arrowhead) and chronic lesions (arrows) cannot be differentiated.

high signal intensity in gray and/or white matter on T2-weighted images. Although vasogenic edema on T2-weighted images typically produces high signal intensity in white matter, the hyperintensity can involve adjacent gray matter. Consequently, posterior leukoencephalopathy can sometimes mimic infarction of the posterior cerebral artery. Hyperperfusion syndrome after carotid endarterectomy can resemble infarction of the middle cerebral artery. Human immunodeficiency virus encephalopathy can produce lesions in a variety of distributions, some of which have a manifestation similar to that of arterial infarction. Deep venous thrombosis can produce bilateral thalamic hyperintensity that is indistinguishable from “top of the basilar” syndrome arterial infarction.

DW MR imaging can be used to reliably distinguish vasogenic from cytotoxic edema. Whereas cytotoxic edema is characterized by restricted diffusion, vasogenic edema is characterized by elevated diffusion due to a relative increase in water in the extracellular compartment, where water is more mobile (75–78). On DW MR images, vasogenic

edema may be hypointense to slightly hyperintense, because these images have both T2 and diffusion contributions. When vasogenic edema is hyperintense on DW MR images, it can mimic hyperacute or subacute infarction. On ADC images, cytotoxic edema due to ischemia is always hypointense for 1–2 weeks, and vasogenic edema is always hyperintense. Therefore, DW MR images should always be compared with ADC images.

Correct differentiation of vasogenic from cytotoxic edema affects patient care. Misdiagnosis of vasogenic edema syndrome as acute ischemia could lead to unnecessary and potentially dangerous use of thrombolytics, antiplatelet agents, anticoagulants, and vasoactive agents. Furthermore, failure to correct relative hypertension could result in increased cerebral edema, hemorrhage, seizures, or death. Misinterpretation of acute ischemic infarction as vasogenic edema syndrome would discourage proper treatment with anticoagulants, evaluation for an embolic source, and liberal blood pressure control, which could increase the risk of recurrent brain infarction.

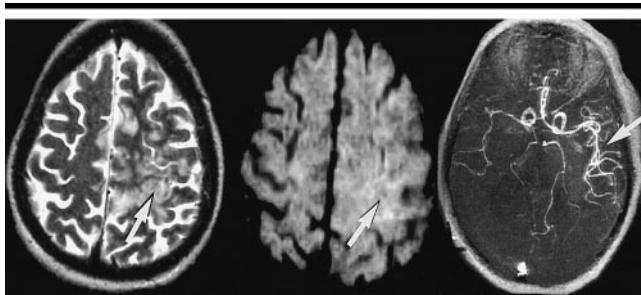


Figure 9. Hyperperfusion syndrome after carotid endarterectomy. The patient developed neurologic symptoms referable to the left hemisphere several days after undergoing a left carotid endarterectomy. The CT scan was abnormal, and the question of infarction was raised. Left: Transverse fast spin-echo T2-weighted MR image (4,000/104; echo train length, eight; matrix, 256 × 192; field of view, 200 × 200 mm; section thickness, 5 mm with 1-mm gap; one signal acquired) demonstrates numerous areas of abnormal high signal intensity (arrow) in the left hemisphere. Infarctions remained in the differential diagnosis. Middle: Transverse DW MR image ($b = 1,000 \text{ sec/mm}^2$; effective gradient, 14 mT/m; 6,000/108; matrix, 256 × 128; field of view, 400 × 200 mm; section thickness, 6 mm with 1-mm gap) reveals predominant isointensity in the left hemisphere with small areas of slight hypointensity and slight hyperintensity (arrow). ADC images (not shown) demonstrated no areas of restricted diffusion. Right: Transverse three-dimensional time-of-flight MR angiogram (49/6.9; 20° flip angle; matrix, 256 × 192; field of view, 200 × 200 mm; section thickness, 1 mm) demonstrates excellent flow-related enhancement (arrow) in the left hemisphere. A diagnosis of hyperperfusion syndrome with vasogenic edema was established on the basis of DW imaging findings. The patient was treated conservatively and recovered fully.

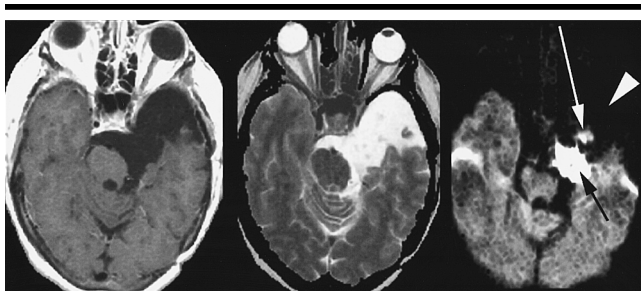


Figure 10. Postoperative residual epidermoid tumor. The patient underwent resection of a large left middle cranial fossa epidermoid tumor that extended into the posterior fossa. Transverse T1-weighted (left) (650/16; matrix, 256 × 192; field of view, 200 × 200 mm; section thickness, 5 mm with 1-mm gap; one signal acquired) and fast spin echo T2-weighted (middle) (4,000/104; echo train length, eight; matrix, 256 × 192; field of view, 200 × 200 mm; section thickness, 5 mm with 1-mm gap, one signal acquired) MR images do not allow clear differentiation of residual mass from the resection cavity. Right: Transverse DW MR image ($b = 1,000 \text{ sec/mm}^2$; effective gradient, 14 mT/m; 6,000/108; matrix, 256 × 128; field of view, 400 × 200 mm; section thickness, 6 mm with 1-mm gap) clearly demonstrates a hyperintense mass (black arrow) adjacent to the left pons and a smaller amount of mass (white arrow) in the left middle cranial fossa, consistent with residual epidermoid tumor. CSF (arrowhead) in the resection cavity is markedly hypointense.

Masses

Extraaxial masses: arachnoid cyst versus epidermoid tumor.—Conventional MR images cannot be used to reliably distinguish epidermoid tumors from arachnoid

cysts; both lesions are very hypointense relative to brain parenchyma on T1-weighted MR images and very hyperintense on T2-weighted images. Epidermoid tumors are solid masses, however, which demonstrate ADCs similar to

those of gray matter and lower than those of CSF (79,80). With the combination of T2 and diffusion effects, epidermoid tumors are markedly hyperintense compared with CSF and brain tissue on diffusion MR images. Conversely, arachnoid cysts are fluid filled, demonstrate very high ADCs, and appear similar to CSF on DW MR images. Furthermore, on conventional MR images obtained after resection of an epidermoid tumor, the resection cavity and residual tumor may be similarly hypointense on T1-weighted images and hyperintense on T2-weighted images. On DW MR images, the hypointense CSF-containing cavity can easily be differentiated from the residual hyperintense epidermoid tumor (Fig 10).

Intraaxial masses.—A number of investigators (76,81–86) have evaluated DW MR imaging of intraaxial tumors (predominantly gliomas) in animals and humans. It has been demonstrated (76,81,83) that tumor and edema have higher ADCs than does normal brain tissue and that central necrosis has a higher ADC than do tumor, edema, or normal brain tissue. Tien et al (76) demonstrated that enhancing tumors have significantly lower ADCs than does adjacent edema, but Brunberg et al (81) found that there is no significant difference between ADCs of enhancing tumor and edema. Both concluded that the ADC alone cannot be used to differentiate a nonenhancing tumor from adjacent edema. Brunberg et al suggested that both enhancing and nonenhancing tumors can be distinguished from edema because edema has significantly higher indices of diffusion anisotropy when compared with adjacent tumor, presumably due to intact myelin within the edema. Demarcation of tumor from surrounding vasogenic edema with DW MR imaging may be important in determining radiation ports, surgical margins, and biopsy sites. A number of investigators (81,84,85) have demonstrated that DW MR imaging cannot be used to differentiate between high- and low-grade gliomas or between tumor types.

DW MR imaging is also valuable in the assessment of tumor resections that are complicated, in the immediate postoperative period, by acute neurologic deficits. Although both extracellular edema and infarction are hyperintense on spin-echo T2-weighted images, cytotoxic edema is characterized by a low ADC, and vasogenic edema is characterized by a high ADC, relative to brain parenchyma. Thus, an acute infarction can easily be differentiated from postoperative edema.

Intracranial Infections

Pyogenic infection.—Abscess cavities and empyemas are homogeneously hyperintense on DW MR images (Fig 11), with signal intensity ratios of abscess cavity to normal brain tissue that range from 2.5 to 6.9 and with ADC ratios that range from 0.36 to 0.46 (87–89). In one study (88), the ADC of the abscess cavity in vivo was similar to that of pus aspirated from the cavity in vitro. In another study (89), the ADC ratio of empyema compared with CSF was 0.13 in one patient. The relatively restricted diffusion most likely results from the high viscosity and cellularity of pus.

Although intracranial abscesses and intracranial neoplasms may appear similar on images obtained with conventional MR sequences, the signal intensity of the abscess cavity is markedly higher and the ADC ratios are lower than those of necrotic tumors on DW MR images (76,81,87). Bacterial meningitis may be complicated by subdural effusions or subdural empyemas, which are difficult to differentiate on conventional MR images. Empyemas are hyperintense on DW MR images and have a restricted ADC, whereas sterile effusions are hypointense and have an ADC similar to that of CSF. Thus, DW MR images may be important when deciding whether to drain or conservatively manage extraaxial collections associated with meningitis.

Herpes encephalitis.—Herpes encephalitis lesions are characterized by marked hyperintensity on DW MR images (Fig 12), with ADC ratios of these lesions to normal brain parenchyma ranging from 0.48 to 0.66. On follow-up conventional T1-weighted and T2-weighted MR images, these areas demonstrate encephalomalacic change. The restricted diffusion is explained by cytotoxic edema in tissue undergoing necrosis. DW MR imaging may aid in distinguishing herpes lesions from infiltrative temporal lobe tumors because the ADCs of herpes lesions are low while the ADCs of various tumors are elevated or in the normal range (76,81).

Creutzfeldt-Jakob disease.—DW MR images in patients with Creutzfeldt-Jakob disease have demonstrated hyperintense lesions in the cortex and basal ganglia (Fig 13). ADCs in lesions in five patients were significantly lower than those of normal brain parenchyma (90,91), while ADCs in lesions in two patients were normal or mildly elevated (92). The variable ADCs are likely related to vari-

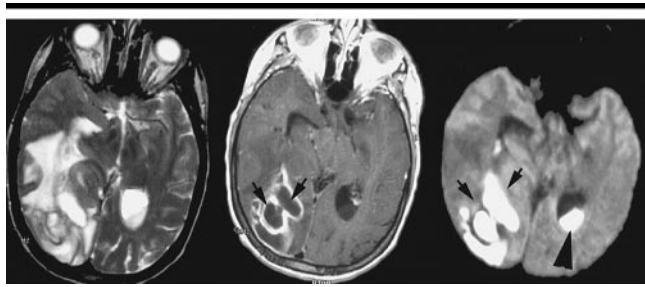


Figure 11. Pathologically proved cerebral abscess. Left: A complex signal intensity pattern is visible in the right occipital and temporal lobes on the fast spin-echo T2-weighted MR image (4,000/104; echo train length, eight; matrix, 256×192 ; field of view, 200×200 mm; section thickness, 5 mm with 1-mm gap; one signal acquired). Middle: Ring-enhancing lesion (arrows) in the right occipital lobe is demonstrated on the gadolinium-enhanced T1-weighted MR image (650/16; matrix, 256×192 ; field of view, 200×200 mm; section thickness, 5 mm with 1-mm gap; one signal acquired). Right: DW MR image ($b = 1,000$ sec/mm²; effective gradient, 14 mT/m; 6,000/108; matrix, 256×128 ; field of view, 400×200 mm; section thickness, 6 mm with 1-mm gap) demonstrates the characteristic restricted diffusion of pyogenic abscess (arrows). Note the hyperintensity (arrowhead) in the left occipital horn due to a loculated collection of pus in this location.

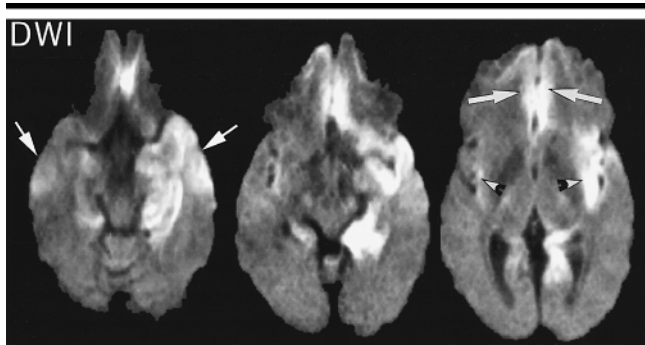


Figure 12. Herpes encephalitis proved with results of polymerase chain reaction test. DW MR images (DWI; $b = 1,000$ sec/mm²; effective gradient, 14 mT/m; 6,000/108; matrix, 256×128 ; field of view, 400×200 mm; section thickness, 6 mm with 1-mm gap) demonstrate restricted diffusion bilaterally in the temporal lobes (short arrows), inferior frontal lobes (long arrows), and insulae (arrowheads), which is a typical distribution for herpes encephalitis.

able amounts of spongiform change, neuronal loss, and gliosis.

Whereas Creutzfeldt-Jakob disease is classically characterized by progressive dementia, myoclonic jerks, and periodic sharp-wave electroencephalographic activity, these features frequently are absent, and Creutzfeldt-Jakob disease cannot be clinically distinguished from other dementing illnesses (93,94). Furthermore, conventional MR images may be normal in as many as 21% of patients (95). Thus, DW MR imaging may be useful for help in the diagnosis of Creutzfeldt-Jakob disease and in the differentiation from Alzheimer disease.

Trauma

Results of an experimental study (96) of head trauma have demonstrated that moderate fluid-percussion injury leads to increased diffusion, reflecting increased extracellular water, in rat cortex and hippocampus. This correlates with a report (97) that moderate fluid-percussion injury does not reduce cerebral blood flow enough to induce ischemia. Ito et al (98) demonstrated no significant change in brain ADCs when rats are subjected to impact acceleration trauma alone. However, when trauma is coupled with hypoxia and hypotension, the ADCs in rat cortex and thalami decrease significantly

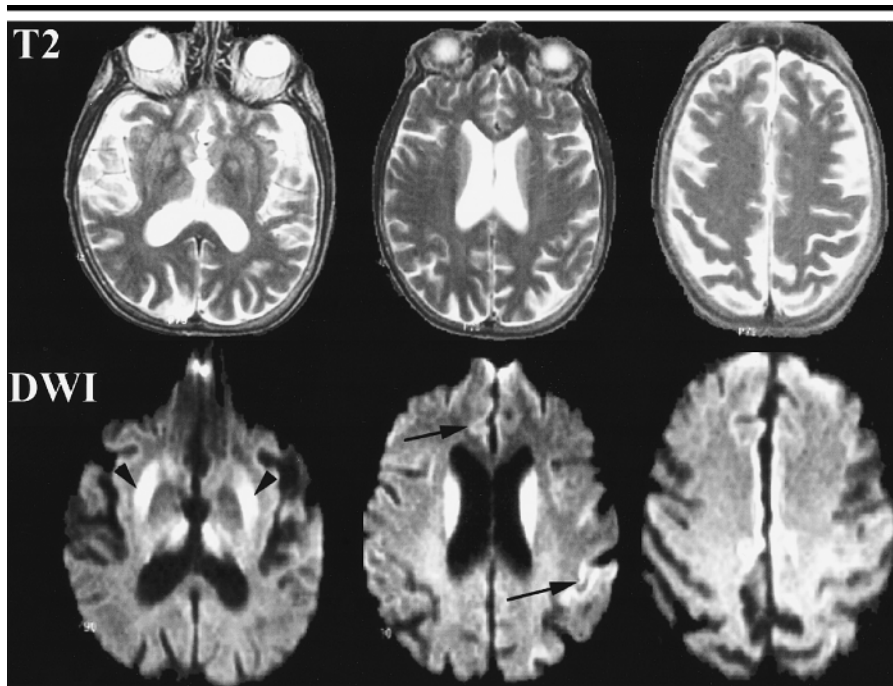


Figure 13. Pathologically proved Creutzfeldt-Jakob disease. Top: Transverse T2-weighted MR images (4,000/104; echo train length, eight; matrix, 256×192 ; field of view, 200×200 mm; section thickness, 5 mm with 1-mm gap; one signal acquired) demonstrate hyperintensity of the basal ganglia. Bottom: Transverse DW MR images (DWI; $b = 1,000$ sec/mm²; effective gradient, 14 mT/m; 6,000/108; matrix, 256×128 ; field of view, 400×200 mm; section thickness, 6 mm with 1-mm gap) show marked hyperintensity involving the basal ganglia bilaterally (arrowheads) and portions of the bilateral cortical ribbon (arrows).

and neuronal injury was observed histologically. They concluded that brain ischemia associated with severe head trauma leads to cytotoxic edema. Barzo et al (99) demonstrated a reduction in rat brain ADCs hours to weeks after an impact acceleration injury. They concluded that cerebral blood flow does not decrease enough to cause ischemic edema and that neurotoxic edema causes the reduced ADCs and neuronal injury.

DW MR imaging in 116 diffuse axonal injury lesions in humans (100) demonstrated changes similar to those in animal models: ADCs were reduced in 64% of lesions, were elevated in 34%, and were similar to ADCs of normal brain tissue in 12%. In addition, most lesions were more conspicuous on DW MR images than on conventional T2-weighted images (Fig 14). Thus, DW MR imaging may be important for the prospective determination of the extent of traumatic injury, the degree of irreversible injury (number of lesions characterized by low ADCs indicative of cytotoxic edema), and the long-term prognosis.

Hemorrhage

The appearance of hemorrhage on DW MR images is complex and involves

many factors, including the relative amounts of different hemorrhagic products and the pulse sequence used (Fig 15). Oxyhemoglobin is hyperintense on DW images and has a lower ADC than does normal brain tissue; this may indicate the relative restriction of water movement inside the red blood cell (101). Extracellular methemoglobin has a higher ADC than does normal brain tissue, which indicates that the mobility of water in the extracellular space is increased. The prolongation of the T2 component of fluid with extracellular methemoglobin results in hyperintensity on DW images. Hemorrhage containing deoxyhemoglobin, intracellular methemoglobin, and hemosiderin are hypointense on DW images because of magnetic susceptibility effects. Because these products of hemorrhage have very low signal intensity on T2-weighted images, ADCs cannot be reliably calculated for them.

Demyelination

Multiple sclerosis.—In animals with experimental allergic encephalomyelitis (a model of multiple sclerosis) and in patients with multiple sclerosis, most plaques demonstrate increased diffusion (102–106). In humans, acute plaques have signifi-

cantly higher ADCs than do chronic plaques (105,106). The elevated diffusion may result from an increase in the size of the extracellular space due to edema and demyelination acutely and to axonal loss and gliosis chronically. In rare instances, acute plaques have restricted diffusion. This may result from increased inflammatory cellular infiltration with little extracellular edema. Of interest, normal-appearing white matter has a mildly increased ADC (104). This correlates with histologic results in which multiple sclerosis was shown to diffusely affect white matter (107).

In monkeys with experimental allergic encephalomyelitis, Heide et al (102) demonstrated that diffusion anisotropy decreased over time. We have also observed this phenomenon in humans. Furthermore, Verhoye et al (103) demonstrated a significant positive correlation between the degree of ADC elevation in the external capsule and severity of clinical disease in rats with experimental allergic encephalomyelitis. However, this relationship has not been confirmed in humans. Horsfield et al (104) demonstrated that benign multiple sclerosis lesions have ADCs similar to those of secondary progressive multiple sclerosis. Furthermore, the degree of ADC elevation within individual lesions did not correlate with the degree of patient disability.

Acute disseminated encephalomyelitis.—Acute disseminated encephalomyelitis lesions have ADCs higher than those of normal white matter, likely as a result of demyelination and increased extracellular water. DW MR imaging cannot help distinguish between multiple sclerosis and acute disseminated encephalomyelitis lesions because both usually have elevated diffusion. Because acute infarctions are characterized by restricted diffusion, however, DW MR imaging should be reliable for help in the differentiation between demyelinating lesions and stroke.

CONCLUSION

The DW MR pulse sequence is a valuable technique. It provides information on the physiologic state of the brain and is particularly sensitive to ischemic infarction. We recommend its use when there is an acute neurologic deficit. As DW imaging improves and becomes more widespread, it is expected to play a greater role in the diagnosis of hyperacute and acute stroke and in the differentiation of stroke from other disease processes that mani-

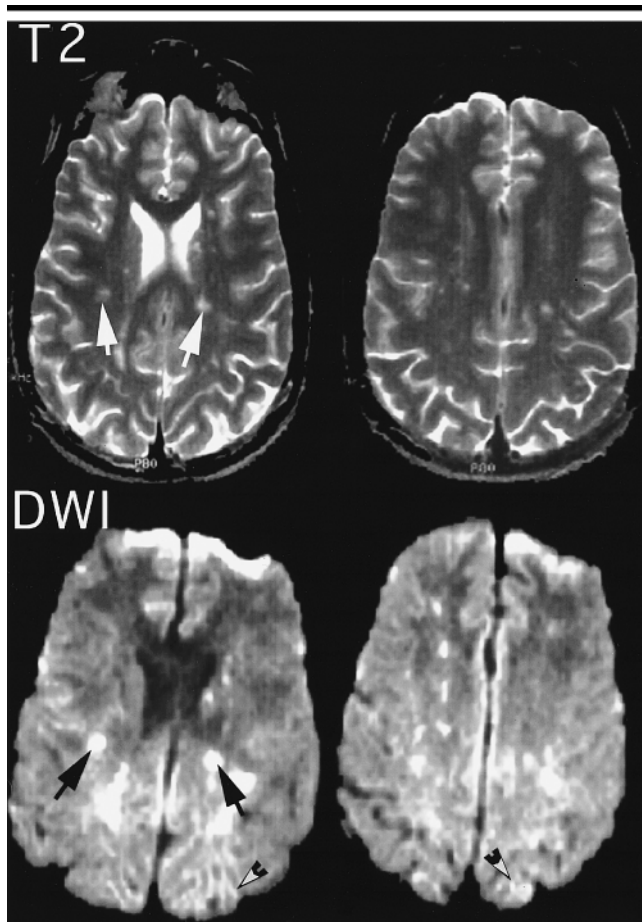


Figure 14. Severe head trauma resulting in diffuse axonal injury. Top: Transverse T2-weighted MR images (4,000/104; echo train length, eight; matrix, 256 × 192; field of view, 200 × 200 mm; section thickness, 5 mm with 1-mm gap; one signal acquired) demonstrate multiple white matter hyperintensities (arrows). Bottom: Transverse DW MR images (DWI; $b = 1,000 \text{ sec/mm}^2$; effective gradient, 14 mT/m; 6,000/108; matrix, 256 × 128; field of view, 400 × 200 mm; section thickness, 6 mm with 1-mm gap) demonstrate the lesions (arrows) with increased conspicuity. The hyperintensity is consistent with restricted diffusion. Note abnormalities (arrowheads) that extend to the cortex posteriorly.

fest with acute neurologic deficits. DW MR imaging will also play a greater role in the management of stroke and may be helpful in the selection of patients for thrombolysis and in the evaluation of new neuroprotective agents. It may prove to be valuable in the evaluation of a wide variety of other disease processes, as described in this review.

Acknowledgments: The authors thank Nandita Guha-Thakurta, MD, and Cara O'Reilly, BA, for their help in the preparation of this manuscript.

References

- Moseley ME, Wendland MF, Kucharczyk J. Magnetic resonance imaging of diffusion and perfusion. *Top Magn Reson Imaging* 1991; 3:50-67.

- Warach S, Chien D, Li W, Ronthal M, Edelman RR. Fast magnetic resonance diffusion-weighted imaging of acute human stroke. *Neurology* 1992; 42:1717-1723. [Erratum: *Neurology* 1992; 42:2192]
- Hossmann KA, Fischer M, Bockhorst K, Hoehn-Berlage M. NMR imaging of the apparent diffusion coefficient (ADC) for the evaluation of metabolic suppression and recovery after prolonged cerebral ischemia. *J Cereb Blood Flow Metab* 1994; 14:723-731.
- Le Bihan D. Diffusion and perfusion magnetic resonance imaging: applications to functional MRI. New York, NY: Raven, 1995.
- Conturo TE, McKinstry RC, Aronovitz JA, Neil JJ. Diffusion MRI: precision, accuracy and flow effects. *NMR Biomed* 1995; 8:307-332.
- Stejskal E, Tanner J. Spin diffusion measurements: spin echos in the presence of

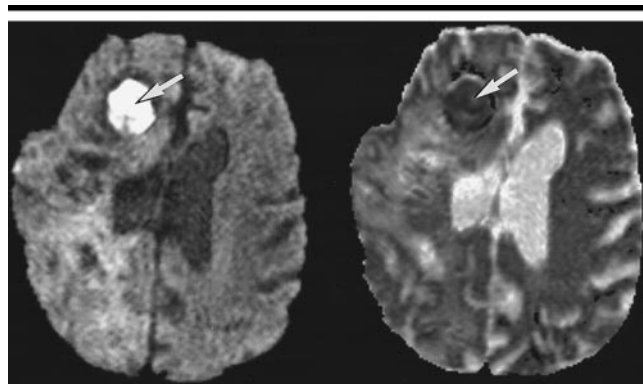


Figure 15. Hematoma in a patient with a right hemisphere glioblastoma who had undergone prior resection and who had developed a hematoma in the right frontal lobe. The patient was hospitalized for progression of symptoms and development of fever. A ring-enhancing lesion at the site of the prior hematoma was seen on a gadolinium-enhanced T1-weighted MR image (not shown) in the right frontal lobe. Left: DW MR image ($b = 1,000 \text{ sec/mm}^2$; effective gradient, 14 mT/m; 6,000/108; matrix, 256 × 128; field of view, 400 × 200 mm; section thickness, 6 mm with 1-mm gap) demonstrates a hyperintense lesion (arrow) in the right frontal lobe. Right: On the ADC image, the lesion is hypointense (arrow), which is consistent with restricted diffusion. The lesion was drained, and old hemorrhage was demonstrated. There was no evidence of infection.

time-dependent field gradient. *J Chem Phys* 1965; 42:288-292.

- Liu G, van Gelderen P, Duyn J, Moonen CT. Single-shot diffusion MRI of human brain on a conventional clinical instrument. *Magn Reson Med* 1996; 35:671-677.
- Baulieu CF, Zhou X, Cofer GP, Johnson GA. Diffusion-weighted MR microscopy with fast spin-echo. *Magn Reson Med* 1993; 30:201-206.
- Gudbjartsson H, Maier SE, Mulkern RV, Morocz IA, Patz S, Jolesz FA. Line scan diffusion imaging. *Magn Reson Med* 1996; 36:509-519.
- Li TQ, Takahashi AM, Hindmarsh T, Moseley ME. ADC mapping by means of a single-shot spiral MRI technique with application in acute cerebral ischemia. *Magn Reson Med* 1999; 41:143-147.
- Brockstedt S, Thomsen C, Wirestam R, Holtas S, Stahlberg F. Quantitative diffusion coefficient maps using fast spin-echo MRI. *Magn Reson Imaging* 1998; 16:877-886.
- de Crespigny AJ, Marks MP, Enzmann DR, Moseley ME. Navigated diffusion imaging of normal and ischemic human brain. *Magn Reson Med* 1995; 33:720-728.
- Nomura Y, Sakuma H, Takeda K, Tagami T, Okuda Y, Nakagawa T. Diffusional anisotropy of the human brain assessed with diffusion-weighted MR: relation with normal brain development and aging. *AJNR Am J Neuroradiol* 1994; 15:231-238.
- Wimberger DM, Roberts TP, Barkovich AJ, Prayer LM, Moseley ME, Kucharczyk J. Identification of "premyelination" by diffusion-weighted MRI. *J Comput Assist Tomogr* 1995; 19:28-33.
- Chien D, Kwong KK, Gress DR, Buonanno FS, Buxton RB, Rosen BR. MR dif-

- fusion imaging of cerebral infarction in humans. *AJNR Am J Neuroradiol* 1992; 13:1097-1102.
16. Mintorovitch J, Yang GY, Shimizu H, Kucharczyk J, Chan PH, Weinstein PR. Diffusion-weighted magnetic resonance imaging of acute focal cerebral ischemia: comparison of signal intensity with changes in brain water and Na⁺,K(+)ATPase activity. *J Cereb Blood Flow Metab* 1994; 14:332-336.
 17. Kucharczyk J, Vexler ZS, Roberts TP, et al. Echo-planar perfusion-sensitive MR imaging of acute cerebral ischemia. *Radiology* 1993; 188:711-717.
 18. Matsumoto K, Lo EH, Pierce AR, Garrido L, Kowall NW. Role of vasogenic edema and tissue cavitation in ischemic evolution on diffusion-weighted imaging: comparison with multiparameter MR and immunohistochemistry. *AJNR Am J Neuroradiol* 1995; 16:1107-1115.
 19. Sevick R, Kanda F, Mintorovitch J, et al. Cytotoxic brain edema: assessment with diffusion-weighted MR imaging. *Radiology* 1992; 185:687-690.
 20. Benveniste H, Hedlund LW, Johnson GA. Mechanism of detection of acute cerebral ischemia in rats by diffusion-weighted magnetic resonance microscopy. *Stroke* 1992; 23:746-754.
 21. Schuier G, Tigges A, Reimer P, Daldrup H, Peters P. The repeatability of MR perfusion studies: a clinical study (abstr). In: Proceedings of the Third Meeting of the International Society for Magnetic Resonance in Medicine. Berkeley, California: International Society for Magnetic Resonance in Medicine, 1995; 84.
 22. Niendorf T, Dijkhuizen R, Norris D, Campagne M, Nicolay K. Biexponential diffusion attenuation in various states of brain tissue: implications for diffusion weighted imaging. *Magn Reson Med* 1996; 847-857.
 23. Sykova E, Svoboda J, Polak J, Chvatal A. Extracellular volume fraction and diffusion characteristics during progressive ischemia and terminal anoxia in the spinal cord of the rat. *J Cereb Blood Flow Metab* 1994; 14:301-311.
 24. Wick M, Nagatomo Y, Prielmeier F, Frahm J. Alteration of intracellular metabolite diffusion in rat brain in vivo during ischemia and reperfusion. *Stroke* 1995; 26:1930-1934.
 25. van der Toorn A, Dijkhuizen R, Tulleken C, Nicolay K. Diffusion of metabolites in normal and ischemic rat brain measured by localized 1H MRS. *Magn Reson Med* 1996; 36:914-922.
 26. Duong TQ, Ackerman JJ, Ying HS, Neil JJ. Evaluation of extra- and intracellular apparent diffusion in normal and globally ischemic rat brain via 19F NMR. *Magn Reson Med* 1998; 40:1-13.
 27. Morikawa E, Ginsberg M, Dietrich W, et al. The significance of brain temperature in focal cerebral ischemia: histopathological consequences of middle cerebral artery occlusion in the rat. *J Cereb Blood Flow Metab* 1992; 12:380-389.
 28. Le Bihan D, Delannoy J, Levin RL. Temperature mapping with MR imaging of molecular diffusion: application to hyperthermia. *Radiology* 1989; 171: 853-857.
 29. Helpert J, Ordidge R, Knight R. The effect of cell membrane water permeability on the apparent diffusion coefficient of water (abstr). In: Book of abstracts: Society of Magnetic Resonance in Medicine 1992. Berkeley, Calif: Society of Magnetic Resonance in Medicine, 1992; 12.
 30. Szafer A, Zhong J, Gore J. Theoretical model for water diffusion in tissues. *Magn Reson Med* 1995; 33:697-712.
 31. Kucharczyk J, Mintorovitch J, Asgari H, Moseley M. Diffusion/perfusion MR imaging of acute cerebral ischemia. *Magn Reson Med* 1991; 19:311-315.
 32. Moseley M, Kucharczyk J, Mintorovitch J, et al. Diffusion-weighted MR imaging of acute stroke: correlation with T2-weighted and magnetic susceptibility-enhanced MR imaging in cats. *AJNR Am J Neuroradiol* 1990; 11:423-429.
 33. Moseley M. Early detection of regional cerebral ischemia in cats: comparison of diffusion- and T2-weighted MRI and spectroscopy. *Magn Reson Med* 1990; 14:330-346.
 34. Mintorovitch J, Moseley M, Chileuitt L, Shimizu H, Cohen Y, Weinstein P. Comparison of diffusion and T2-weighted MRI for the early detection of cerebral ischemia and reperfusion in rats. *Magn Reson Med* 1991; 18:39-50.
 35. Moonen C, Pekar J, Vleeschouwer MD, Van Gelderen P, Zijl PV, DesPres D. Restricted and anisotropic displacement of water in healthy cat brain and in stroke studied by NMR diffusion imaging. *Magn Reson Med* 1991; 19:327-332.
 36. Warach S, Gaa J, Siewert B, Wielopolski P, Edelman R. Acute human stroke studied by whole brain echo planar diffusion-weighted magnetic resonance imaging. *Ann Neurol* 1995; 37:231-241.
 37. Schlaug G, Siewert B, Benfield A, Edelman R, Warach S. Time course of the apparent diffusion coefficient (ADC) abnormality in human stroke. *Neurology* 1997; 49:113-119.
 38. Lutsep H, Albers G, DeCrespigny A, Kamat G, Marks M, Moseley M. Clinical utility of diffusion-weighted magnetic resonance imaging in the assessment of ischemic stroke. *Neurology* 1997; 41:574-580.
 39. Schwamm L, Koroshetz W, Sorensen A, et al. Time course of lesion development in patients with acute stroke: serial diffusion and hemodynamic weighted magnetic resonance imaging. *Stroke* 1998; 29:2268-2276.
 40. Marks M, Tong DC, Beaulieu C, Albers GW, de Crespigny A, Moseley ME. Evaluation of early reperfusion and i.v. tPA therapy using diffusion- and perfusion-weighted MRI. *Neurology* 1999; 52:1792-1798.
 41. Nagesh V, Welch KM, Windham JP, et al. Time course of ADCw changes in ischemic stroke: beyond the human eye! *Stroke* 1998; 29:1778-1782.
 42. Villringer A, Rosen BR, Belliveau JW, et al. Dynamic imaging with lanthanide chelates in normal brain: contrast due to magnetic susceptibility effects. *Magn Reson Med* 1988; 6:164-174.
 43. Rosen BR, Belliveau JW, Aronen HJ, et al. Susceptibility contrast imaging of cerebral blood volume: human experience. *Magn Reson Med* 1991; 22: 293-299.
 44. Ostergaard L, Sorensen AG, Kwong KK, Weisskoff RM, Gyldensted C, Rosen BR. High resolution measurement of cerebral blood flow using intravascular tracer bolus passages. II. Experimental comparison and preliminary results. *Magn Reson Med* 1996; 36:726-736.
 45. Ostergaard L, Weisskoff RM, Chesler DA, Gyldensted C, Rosen BR. High resolution measurement of cerebral blood flow using intravascular tracer bolus passages. I. Mathematical approach and statistical analysis. *Magn Reson Med* 1996; 36:715-725.
 46. Rosen BR, Belliveau JW, Vevea JM, Brady TJ. Perfusion imaging with NMR contrast agents. *Magn Reson Med* 1990; 14: 249-265.
 47. Rosen BR, Belliveau JW, Buchbinder BR, et al. Contrast agents and cerebral hemodynamics. *Magn Reson Med* 1991; 19:285-292.
 48. Quast M, Huang N, Hillman G, Kent T. The evolution of acute stroke recorded by multimodal magnetic resonance imaging. *Magn Reson Imaging* 1993; 11: 465-471.
 49. Baird A, Benfield A, Schlaug G, et al. Enlargement of human cerebral ischemic volumes measured by diffusion-weighted magnetic resonance imaging. *Ann Neurol* 1997; 41:581-589.
 50. Rordoff G, Koroshetz W, Copen W, et al. Regional ischemia and ischemic injury in patients with acute middle cerebral artery stroke as defined by early diffusion-weighted and perfusion-weighted MRI. *Stroke* 1998; 29:939-943.
 51. Barber P, Darby D, Desmond P, et al. Prediction of stroke outcome with echoplanar perfusion- and diffusion-weighted MRI. *Neurology* 1998; 51:418-456.
 52. Sorensen A, Buonanno F, Gonzalez R, et al. Hyperacute stroke: evaluation with combined multisection diffusion-weighted and hemodynamically weighted echo-planar MR imaging. *Radiology* 1996; 199:391-401.
 53. Tatlisumak T, Carano R, Takano K, Ogenorth T, Sotak C, Fisher M. A novel endothelin antagonist, A-127722, attenuates ischemic lesion size in rats with temporary middle cerebral artery occlusion. *Stroke* 1998; 29:850-858.
 54. Minematsu K, Fisher M, Li L, et al. Effects of novel NMDA antagonist on experimental stroke rapidly and quantitatively assessed by diffusion-weighted MRI. *Neurology* 1993; 43:397-403.
 55. Hasegawa Y, Fisher M, Latour L, Dardzinski B, Sotak C. MRI diffusion mapping of reversible and irreversible ischemic injury in focal brain ischemia. *Neurology* 1994; 44:1484-1490.
 56. Muller TB, Haraldseth O, Jones RA, et al. Combined perfusion and diffusion-weighted magnetic resonance imaging in a rat model of reversible middle cerebral artery occlusion. *Stroke* 1995; 26: 451-457.
 57. Minematsu K, Li L, Sotak C, Davis M, Fisher M. Reversible focal ischemic injury demonstrated by diffusion-weighted magnetic resonance imaging. *Stroke* 1992; 23:1304-1310.
 58. Dardzinski B, Sotak C, Fisher M, Hasegawa Y, Li L, Minematsu K. Apparent diffusion coefficient mapping of ex-

- perimental focal cerebral ischemia using diffusion-weighted echo-planar imaging. *Magn Reson Med* 1993; 30:318-325.
59. Marks MP, De Crespigny A, Lentz D, Enzmann DR, Albers GW, Moseley ME. Acute and chronic stroke: navigated spin-echo diffusion-weighted MR imaging. *Radiology* 1996; 199:403-408.
 60. Gonzalez RG, Schaefer PW, Buonanno FS, et al. Diffusion-weighted MR imaging: diagnostic accuracy in patients imaged within 6 hours of stroke symptom onset. *Radiology* 1999; 210:155-162.
 61. Mohr J, Biller J, Hial S, et al. Magnetic resonance versus computed tomographic imaging in acute stroke. *Stroke* 1995; 26:807-812.
 62. Bryan R, Levy L, Whitlow W, Killian J, Preziosi T, Rosario J. Diagnosis of acute cerebral infarction: comparison of CT and MR imaging. *AJNR Am J Neuroradiol* 1991; 12:611-620.
 63. Lovblad K, Laubach H, Baird A, et al. Clinical experience with diffusion-weighted MR in patients with acute stroke. *AJNR Am J Neuroradiol* 1998; 19:1061-1066.
 64. Singer M, Chong J, Lu D, Schonewille W, Tuhim S, Atlas S. Diffusion-weighted MRI in acute subcortical infarction. *Stroke* 1998; 29:133-136.
 65. Ay H, Buonanno FS, Rordorf G, et al. Normal diffusion-weighted MRI during stroke-like deficits. *Neurology* 1999; 52:1784-1792.
 66. Lovblad K, Baird A, Schlaug G, et al. Ischemic lesion volumes in acute stroke by diffusion-weighted magnetic resonance imaging correlate with clinical outcome. *Ann Neurol* 1997; 42:164-170.
 67. Tong D, Yenari M, Albers G, O'Brien M, Marks M, Moseley M. Correlation of perfusion- and diffusion-weighted MRI with NIHSS score in acute (<6.5 hour) ischemic stroke. *Neurology* 1998; 50:864-870.
 68. van Everdingen KJ, van der Grond J, Kapelle LJ, Ramos LM, Mali WP. Diffusion-weighted magnetic resonance imaging in acute stroke. *Stroke* 1998; 29:1783-1790.
 69. Tuor U, Kozlowski P, Bigio MD, Ramjiawan B, Su S, Maliszka K. Diffusion- and T2-weighted increases in magnetic resonance images of immature brain during hypoxia-ischemia: transient reversal post hypoxia. *Neurology* 1998; 150:321-328.
 70. D'Arceuil HE, de Crespigny AJ, Rother J, et al. Diffusion and perfusion magnetic resonance imaging of the evolution of hypoxic ischemic encephalopathy in the neonatal rabbit. *J Magn Reson Imaging* 1998; 8:820-828.
 71. Cowan FM, Pennock JM, Hanrahan JD, Manji KP, Edwards AD. Early detection of cerebral infarction and hypoxic ischemic encephalopathy in neonates using diffusion-weighted magnetic resonance imaging. *Neuropediatrics* 1994; 25:172-175.
 72. Phillips MD, Zimmerman RA. Diffusion imaging in pediatric hypoxic ischemia injury. *Neuroimaging Clin N Am* 1999; 9:41-52.
 73. Ay H, Buonanno F, Schaefer P, et al. Clinical and diffusion-weighted imaging characteristics of an identifiable subset of TIA patients with acute infarction (abstr). In: CD-ROM book of abstracts: 24th American Heart Association International Conference on Stroke and Cerebral Circulation. Dallas, Tex: American Heart Association, 1999.
 74. Kidwell CS, Alger JR, DiSalle F, et al. Diffusion MRI in patients with transient ischemic attacks. *Stroke* 1999; 30:1174-1180.
 75. Ebisu T, Naruse S, Horikawa Y, et al. Discrimination between different types of white matter edema with diffusion-weighted MR imaging. *J Magn Reson Imaging* 1993; 3:863-868.
 76. Tien R, Felsberg G, Friedman H, Brown M, MacFall J. MR imaging of high-grade cerebral gliomas: value of diffusion-weighted echoplanar pulse sequences. *AJR Am J Roentgenol* 1994; 162:671-677.
 77. Schaefer P, Buonanno F, Gonzalez R, Schwamm L. Diffusion weighted imaging discriminates between cytotoxic and vasogenic edema in a patient with eclampsia. *Stroke* 1997; 28:1-4.
 78. Schwartz R, Mulker R, Gudbjartsson H, Jolesz F. Diffusion-weighted MR imaging in hypertensive encephalopathy: clues to pathogenesis. *AJNR Am J Neuroradiol* 1998; 19:859-862.
 79. Tsuruda J, Chew W, Moseley M, Norman D. Diffusion-weighted MR imaging of the brain: value of differentiating between extra-axial cysts and epidermoid tumors. *AJNR Am J Neuroradiol* 1990; 11:925-931.
 80. Maeda M, Kawamura Y, Tamagawa Y, et al. Intravoxel incoherent motion (IVIM) MRI in intracranial, extra-axial tumors and cysts. *J Comput Assist Tomogr* 1992; 16:514-518.
 81. Brunberg J, Chenevert T, McKeever P, et al. In vivo MR determination of water diffusion coefficients and diffusion anisotropy: correlation with structural alteration in gliomas of the cerebral hemispheres. *AJNR Am J Neuroradiol* 1995; 16:361-371.
 82. Eis M, Els T, Hoehn-Berlage M, Houssman K. Quantitative MR imaging of cerebral tumor and edema. *Acta Neurochir* 1994; (suppl):344-346.
 83. Els T, Eis M, Hoehn-Berlage M, Hossman K. Diffusion-weighted imaging of experimental brain tumors in rats. *MAGMA* 1995; 3:13-20.
 84. Aronen H, Cohen M, Belliveau J, Fordham J, Rosen B. Ultrafast imaging of brain tumors. *Top Magn Reson Imaging* 1993; 5:14-24.
 85. Eis M, Els T, Hoehn-Berlage M. High resolution quantitative relaxation and diffusion MRI of three different experimental brain tumors in rats. *Magn Reson Med* 1995; 34:835-844.
 86. Ostergaard L, Hochberg F, Rabinov J, et al. Early changes measured by magnetic resonance imaging in cerebral blood flow, blood volume and blood brain barrier permeability following dexamethasone treatment in patients with brain tumors. *J Neurosurg* 1999; 90:300-305.
 87. Kim Y, Chang K, Kim H, Seong S, Kim Y, Han M. Brain abscess and necrotic or cystic brain tumor: discrimination with signal intensity on diffusion-weighted MR imaging. *AJR Am J Roentgenol* 1998; 171:1487-1490.
 88. Ebisu T, Tanaka C, Umeda M, et al. Discrimination of brain abscess from necrotic or cystic tumors by diffusion-weighted echo planar imaging. *Magn Reson Imaging* 1996; 14:1113-1116.
 89. Schaefer P, Wang B, Gonzalez R. Echo planar diffusion weighted imaging in pyogenic infections (abstr). In: Proceedings of the 35th Annual Meeting of the American Society of Neuroradiology. Oak Brook, Ill: American Society of Neuroradiology, 1997; 103.
 90. Bahn M, Kido D, Lin W, Pearlman A. Brain magnetic resonance diffusion abnormalities in Creutzfeldt-Jakob disease. *Arch Neurol* 1997; 54:1411-1415.
 91. Schaefer P, Grant E, Wang B, Gonzalez R. Echo planar diffusion weighted imaging (DWI) in Creutzfeldt-Jakob disease (CJD) (abstr). In: Proceedings of the 37th Annual Meeting of the American Society of Neuroradiology. Oak Brook, Ill: American Society of Neuroradiology, 1999; 161.
 92. Demaerel P, Heiner L, Robberecht W, Sciot R, Wilms G. Diffusion-weighted MRI in sporadic Creutzfeldt-Jakob disease. *Neurology* 1999; 52:205-208.
 93. Brown P, Cathala F, Castaigne P, Gajdusek DC. Creutzfeldt-Jakob disease: clinical analysis of a consecutive series of 230 neuropathologically verified cases. *Ann Neurol* 1986; 20:597-602.
 94. Johnson R, Gibbs C. Creutzfeldt-Jakob disease and related transmissible spongiform encephalopathies. *N Engl J Med* 1998; 339:1994-2004.
 95. Finkenstaedt M, Szudra A, Zerr I, et al. MR imaging of Creutzfeldt-Jakob disease. *Radiology* 1996; 199:793-798.
 96. Hanstock C, Faden A, Bendall M, Vink R. Diffusion-weighted imaging differentiates ischemic tissue from traumatized tissue. *Stroke* 1994; 25:843-848.
 97. Yuan X, Prough D, Smith T, DeWitt D. The effects of traumatic brain injury in regional cerebral blood flow in rats. *J Neurotrauma* 1988; 5:289-301.
 98. Ito J, Marmarou A, Barzo P, Fatouros P, Corwin F. Characterization of edema by diffusion-weighted imaging in experimental traumatic brain injury. *J Neurosurg* 1996; 84:97-103.
 99. Barzo P, Marmarou A, Fatouros P, Hayasaki K, Corwin F. Contribution of vasogenic and cellular edema to traumatic brain swelling measured by diffusion-weighted imaging. *J Neurosurg* 1997; 87:900-907.
 100. Schaefer P, Tievsky A, Gonzalez R. Echo planar (EP) diffusion weighted imaging (dwi) in diffuse axonal injury (dai) (abstr). In: Proceedings of the 36th Annual Meeting of the American Society of Neuroradiology. Oak Brook, Ill: American Society of Neuroradiology, 1998; 216.
 101. Atlas SW, Dubois P, Singer MB, Lu D. Diffusion measurements in intracranial hematomas: implications for MR imaging of acute stroke. *AJNR Am J Neuroradiol* 2000; 21:1190-1194.
 102. Heide A, Richards T, Alvord E, Peterson J, Rose L. Diffusion imaging of experimental allergic encephalomyelitis. *Magn Reson Med* 1993; 29:478-484.

103. Verhoye MR, 's-Gravenmade EJ, Raman ER, Van Reempts J, Van der Linden A. In vivo noninvasive determination of abnormal water diffusion in the rat brain studied in and animal model for multiple sclerosis by diffusion-weighted NMR imaging. *Magn Reson Imaging* 1996; 14: 521–532.
104. Horsfield M, Lai M, Webb S, et al. Apparent diffusion coefficients in benign and secondary progressive multiple sclerosis by nuclear magnetic resonance. *Magn Reson Med* 1996; 36:393–400.
105. Christiansen P, Gideon P, Thomsen C, Stubgaard M, Henriksen O, Larsson H. Increased water self-diffusion in chronic plaques and in apparently normal white matter in patients with multiple sclerosis. *Acta Neurol Scand* 1993; 87:195–199.
106. Larsson H, Thomsen C, Frederiksen J, Stubgaard M, Henriksen O. In vivo magnetic resonance diffusion measurement in the brain of patients with multiple sclerosis. *Magn Reson Imaging* 1992; 10:7–12.
107. Allen IV, McKeown SR. A histological, histochemical and biochemical study of the macroscopically normal white matter in multiple sclerosis. *J Neurol Sci* 1979; 41:81–91.